AIP | Journal of Applied Physics

Electrical and magnetic properties of chemically derived nanocrystalline cobalt ferrite

N. Sivakumar, A. Narayanasamy, K. Shinoda, C. N. Chinnasamy, B. Jeyadevan et al.

Citation: J. Appl. Phys. **102**, 013916 (2007); doi: 10.1063/1.2752098
View online: http://dx.doi.org/10.1063/1.2752098
View Table of Contents: http://jap.aip.org/resource/1/JAPIAU/v102/i1
Published by the AIP Publishing LLC.

Electrical and magnetic properties of chemically derived nanocrystalline cobalt ferrite

N. Sivakumar and A. Narayanasamy[a)]
Materials Science Centre, Department of Nuclear Physics, University of Madras, Guindy Campus, Chennai 600 025, India

K. Shinoda, C. N. Chinnasamy,[b)] and B. Jeyadevan
Graduate School of Environmental Studies, Tohoku University, Sendai 980-8579, Japan

J.-M. Greneche
Laboratoire de Physique de l'Etat condensé, UMR CNRS 6087, Université du Maine, Faculté des Sciences, 72085 Le Mans Cedex 9, France

(Received 24 November 2006; accepted 23 May 2007; published online 12 July 2007)

Nanocrystalline cobalt ferrite particles of 8 nm grain size were synthesized by coprecipitation technique and subsequently suitably heat treated to obtain higher grain sizes. The experimentally observed changes in the dc electrical conductivity and Curie temperature with heat treatment have been attributed to the changes in the cation distributions as obtained from the Mössbauer and extended x-ray absorption fine structure (EXAFS) measurements and to the grain size. The activation energies for conduction as determined from the Arrhenius plots suggest that the conductivity is due to hopping of both electrons and holes. The observed decrease in conductivity when the grain size is increased from 8 to 92 nm is clearly due to the predominant effect of migration of some of the Fe^{3+} ions from octahedral to tetrahedral sites, as is evident from in-field Mössbauer and EXAFS measurements. But the higher conductivity of the 102 and 123 nm particles compared to that of the 92 nm particles is attributed to the higher grain size, since the cation distribution is found to be the same for all these three samples. The Néel temperature increases from 709 K for the as-prepared particles (8 nm) to 809 K for the 92 nm particles because of the change in the cation distribution and it remains almost the same for the higher grain sizes as there is no further change in the cation distribution. © *2007 American Institute of Physics*.
[DOI: 10.1063/1.2752098]

I. INTRODUCTION

Recent trend in nanotechnology has initiated renewed interest in spinel ferrites in order to explore the possibility of widening the range of their applications. The cation distribution in ferrites has a remarkable effect on the electrical conductivity and magnetic behavior. Interesting results have been reported on the electrical conductivity behavior of $NiFe_2O_4$ and Ni–Zn ferrites.[1,2] The bulk particles of cobalt ferrite normally exhibit inverse spinel structure with one half of Fe^{3+} ions in the *A* sites and the remaining half of Fe^{3+} ions and Co^{2+} ions in the *B* sites.[3] There is an ever increasing interest in cobalt ferrite in the nanometer range because of its extensive application in high-density magnetic recording.[4] Cobalt ferrite with high coercivity is a promising material for various magnetic applications such as magneto-optical devices and magnetic recording.[5–7]

The electrical and magnetic properties of bulk $CoFe_2O_4$ ferrite are found to be sensitive to the distribution of the transition metal ions among the cationic sites in the spinel structure.[8–13] Many researchers have extensively studied the magnetic properties of nanostructured $CoFe_2O_4$.[14–19] Chinnasamy *et al.*[19] have observed a high coercivity of 2.02 kOe at room temperature for $CoFe_2O_4$ particles with a grain size of 36 nm; moreover, the same authors[20] have observed a coercivity value of 4.3 kOe at room temperature for the 40 nm size single domain $CoFe_2O_4$ particles which is close to the theoretical value of 5.3 kOe. Jonker[21] has studied the electrical properties of a series of bulk $Co_{3-x}Fe_xO_4$ ferrites and observed that the conductivity is minimum for the $x=2$ composition and that it is a *p*-type conductor for $x<2$ and an *n*-type conductor for $x>2$. Na *et al.*[22,23] have studied the electrical conduction mechanism of bulk $CoFe_2O_4$ for various heat treatment conditions. They have observed that the electrical resistance of cobalt ferrite decreases with increasing quenching temperature due to the decrease of grain boundary resistance in Fe-excess cobalt ferrites prepared by ceramic method. Wu *et al.*[24] have studied the variation of resistivity with pressure and observed a phase transition from the spinel to tetragonal structure at 7.5 GPa for the 6 nm grain size cobalt ferrite. However, there is no detailed study available in literature on the electrical conductivity behavior of nanostructured $CoFe_2O_4$. This has motivated us to study the effect of grain size on the electrical conductivity and Néel temperature of cobalt ferrite in the nanoregime. The cation distribution, determined by using extended x-ray absorption fine structure (EXAFS) and Mössbauer techniques,

[a)]Electronic mail: ansjourn@rediffmail.com
[b)]Present address: Department of Electronic and Computer Engineering, Northeastern University, 360 Huntington Avenue, Boston Massachusetts 02115.

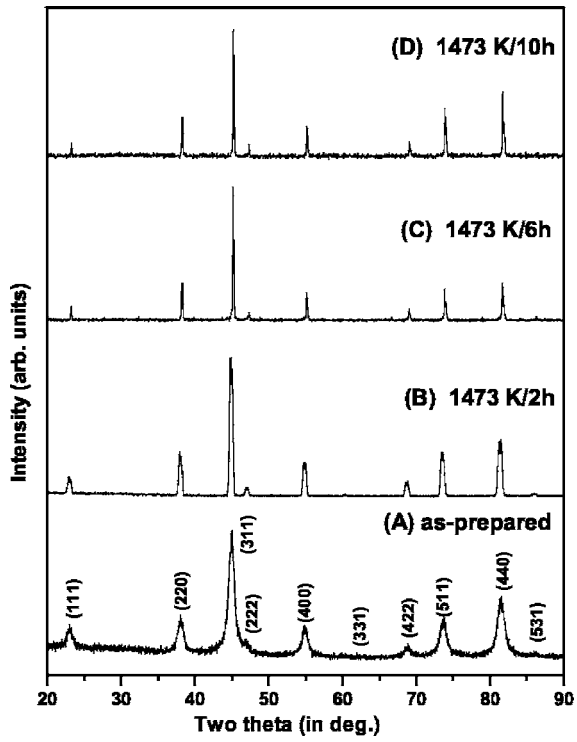

FIG. 1. XRD patterns of $CoFe_2O_4$ spinel samples: (A) as-prepared, and annealed at 1473 K for (B) 2 h, (C) 6 h, and (D) 10 h.

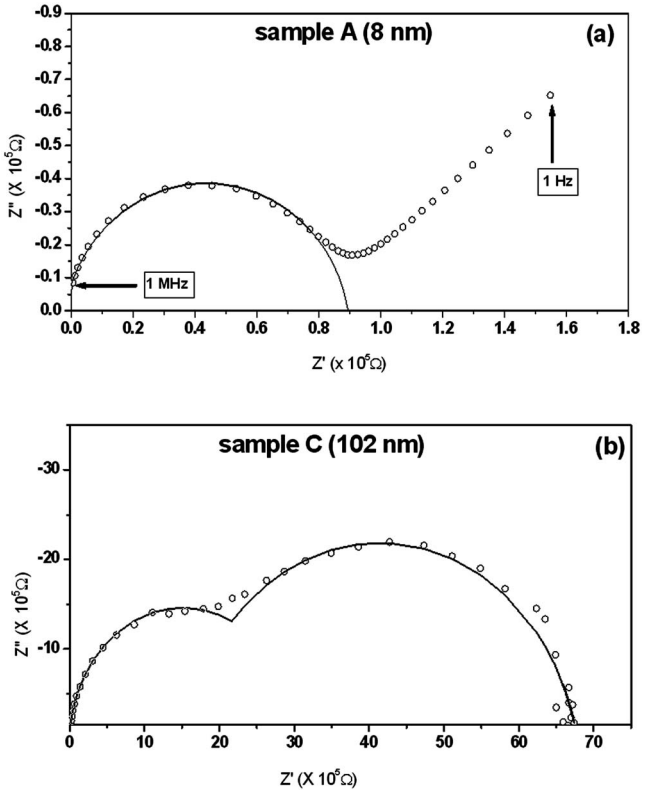

FIG. 2. (a) Complex impedance spectrum of sample *A* measured at 298 K. The continuous curve is the fitted semicircle. (b) The complex impedance spectrum of $CoFe_2O_4$ for sample *C* measured at 448 K. The continuous curves are the fitted semicircles.

is also shown to play a decisive role on the electrical conductivity and Néel temperature of these ferrites.

II. EXPERIMENT

The $CoFe_2O_4$ ferrite was prepared using the conventional coprecipitation technique as reported in our earlier paper.[20] To achieve various grain sizes, the as-prepared sample was heat treated at 1473 K for different durations such as 2, 6, and 10 h. The phase analysis for the as-prepared and heat treated samples was carried out using x-ray diffraction (XRD) with a Rigaku-make high precision Guinier x-ray diffractometer and Fe K_α radiation. The average grain size was determined from the full width at half maximum of the (311) reflection of the XRD patterns using Scherrer's formula.[25] The electrical conductivity measurements were carried out using an impedance analyzer (Solatron 1260 impedance/gain-phase analyzer) in the temperature range of 298–650 K and in the frequency range of 1 Hz–10 MHz. For these measurements, the sample was made in the form of a pellet with 8 mm diameter. The sample was sandwiched between two platinum electrodes of 10 mm diameter. Before starting the measurements, the sample was preheated to 450 K for 15 min to remove the moisture content. The EXAFS measurements were done using a laboratory x-ray absorption spectrometer (Rigaku R-XAS Lopper) at Fe *K* and Co *K* absorption edges. The x-ray beam was generated from the demountable x-ray tube with Mo target as the x-ray source which was monochromatized by the Johansson-type single crystal Ge (220) monochromator. The ^{57}Fe Mössbauer spectra were recorded at 15 K with 8 T magnetic field applied parallel to the direction of gamma rays. The Néel temperature was determined using a thermogravimetric analyzer (Perkin-Elmer series 7) by applying a small magnetic field of 4 mT using a horseshoe magnet.

III. RESULTS AND DISCUSSION

A. Structural analysis

Figure 1 shows the XRD patterns of the as-prepared sample (*A*), sample annealed at 1473 K/2 h (*B*), (c) annealed at 1473 K/6 h (*C*), and annealed at 1473 K/10 h (*D*). All the peaks in Fig. 1 could be indexed to single spinel phase. The increase in grain size with heat treatment is clearly observed from the decrease in the width of the XRD lines. The average grain sizes were calculated using Scherrer's formula taking into account the instrumental line broadening. The average grain sizes of samples *A*–*D* were 8, 92, 102, and 123 nm, respectively. Annealing at 1473 K for 6 and 10 h was carried out to have a grain size variation but without altering the cation distribution in order to study the effect of grain size alone on the electrical properties.

B. dc conductivity

Figure 2(a) shows the impedance plot of the as-prepared sample (sample *A*). The plot consists of only one semicircle, which represents the grain boundary contribution to conductivity. Similarly the impedance plot consists of only one semicircle for the sample *B* also which is not shown in figure. But in the case of samples *C* and *D* the impedance plots consist of two semicircles arising from the grain and grain

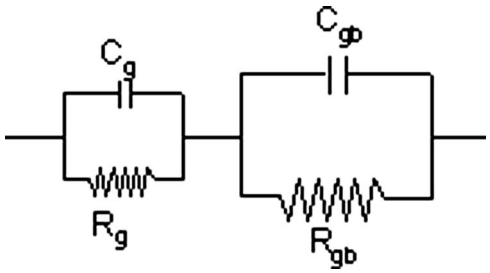

FIG. 3. Proposed model for the impedance behavior where C_g is the bulk capacitance, R_g is the bulk resistance, C_{gb} is the grain boundary capacitance, and R_{gb} is the grain boundary resistance.

boundary contributions as shown in Fig. 2(b) for sample *C*. The equivalent circuit based on the impedance data for samples *C* and *D* is shown in Fig. 3. The parameters R_g and C_g correspond to the resistance and capacitance of the grain, respectively, and R_{gb} and C_{gb} are the corresponding quantities for the grain boundary. The grain and grain boundary resistances were obtained by analyzing the impedance data using the nonlinear least-squares (NLLS) fitting routine. For sample *A*, the grain boundary volume is high because of the small grain sizes and hence the conduction takes place predominantly through the grain boundary and hence a single semicircle is obtained in the impedance plot. In the case of samples *C* and *D* the grain boundary volume should be smaller and hence the conduction takes place through both grain and grain boundary. Even though the grain boundary volume fraction is small for sample *B*, the occurrence of a single semicircle in the impedance plot suggests that the grain and grain boundary have equal resistances. The dc conductivity values were calculated from the resistance values and using the geometrical dimensions of the samples.

Figure 4 shows the Arrhenius plots for the electrical conductivity of the as-prepared and heat treated samples, plotted in the temperature range from 475 to 625 K. The conductivity increases with temperature as expected from the semiconducting behavior of spinel ferrites. For all the samples there

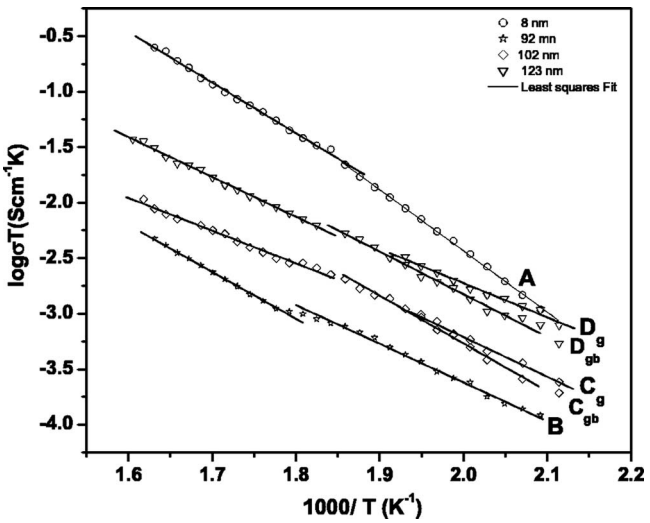

FIG. 4. Arrhenius plots for the electrical conductivity of nanocrystalline $CoFe_2O_4$ spinel samples. The solid lines are the least-squares fit to Eq. (1) (*g*: grain; gb: grain boundary).

TABLE I. The values of activation energies for electrical conductivity in $CoFe_2O_4$ spinel ferrite samples. E_a is the activation energy obtained from the conductivity data for the low-temperature region and E_a' is for the high-temperature region. E_p is the activation energy obtained from the hopping frequency for the low-temperature region and E_p' is for the high-temperature region.

Sample (grain size in nanometer)	Activation energy for grain boundary from the conductivity data		Activation energy from hopping frequency	
	E_a (eV) [±0.01]	E_a' (eV) [±0.01]	E_p (eV) [±0.01]	E_p' (eV) [±0.01]
A (8)	1.09	0.89	1.06	0.73
B (92)	0.66	0.84	0.55	0.72
C (102)	0.63	0.54	0.73	0.57
D (123)	0.75	0.71	0.58	0.60

is a change in the slope of the straight lines at about a temperature of 540±3 K, which is much below their Néel temperatures. The change of slope in the Arrhenius plot, therefore, indicates that there are two different thermally activated processes in the conduction process. The values of activation energies obtained in the present study also suggest that the hopping of charge carriers is responsible for the electrical conductivity. The activation energy for the thermally activated hopping process was obtained by fitting the dc conductivity data with the Arrhenius relation,

$$\sigma T = \sigma_0 \exp\left(-\frac{E_a}{k_B T}\right), \tag{1}$$

where σ_0 is the preexponential factor with the dimensions of $(\Omega\ \mathrm{cm})^{-1}$ K, E_a is the activation energy for dc conductivity, and k_B is the Boltzmann constant and the values of activation energies for grain boundary conduction are given in Table I for all samples. The activation energy E_a for the grain conduction in samples *C* and *D* were obtained as 0.70 and 0.61 eV, respectively. Figure 4 shows that the conductivity decreases when the grain size increases from 8 to 92 nm whereas it is expected to increase with the grain size. There should be, therefore, some other factor for the observed decrease in conductivity. The possible change in cation distribution on annealing at 1473 K for 2 h might have contributed to the observed decrease in the conductivity. The in-field Mössbauer and EXAFS measurements gave a clear evidence for the migration of some of the Fe^{3+} ions from the octahedral to tetrahedral sites and some of the Co^{2+} ions in the reverse direction as discussed in detail in Sec. III F and III G, respectively. In cobalt ferrites, the hopping of both electrons and holes contributes to the electrical conductivity. The electrons and holes are derived from Fe^{2+} ions and Co^{3+} ions, which could be present only in octahedral sites from the crystal field stabilization energy point of view. The decrease in the number of iron ions in octahedral site will result in the decrease of $Fe^{2+} \leftrightarrow Fe^{3+}$ pairs contributing to the decrease in conductivity. Even though the number of holes taking part in conduction increases as the number of $Co^{3+} \leftrightarrow Co^{2+}$ pairs in the octahedral sites increases, due to the migration of some of the cobalt ions from the tetrahedral sites to octahedral

sites, the overall conductivity decreases because of the smaller mobility of holes compared to the electron mobility. When the annealing duration is further increased to 6 and 10 h, the conductivity also increases. However, the cation distribution does not change for these two samples and it almost remains the same as that for the 2 h annealed sample. The increase in conductivity, therefore, can be attributed to the higher grain sizes when the grain to grain contact is expected to be enhanced.

The temperatures at which the slopes of the straight lines in the Arrhenius plot change are below the measured Néel temperatures of these samples as reported in Sec. III H. Therefore, the effect of magnetic state of the ferrites is ruled out for the change of slope in the Arrhenius plots. Moreover, the activation energy for conductivity in the high temperature region is significantly smaller than that for the low temperature region in the case of sample *A*, almost equal for sample *D*, slightly smaller for sample *C* but higher in the case of sample *B*. As the mobility of charge carriers is temperature dependent, an increase in the mobility might have caused a reduction in the activation energy in the high temperature region. Mahajan *et al.*[26] also have obtained similar results. Their explanation is that at low temperatures the conduction is due to hole hopping between $Co^{3+} \leftrightarrow Co^{2+}$ pairs and that because of the low mobility of holes the activation energy is higher in the low temperature region. At higher temperatures the majority charge carriers are electrons due to oxidation reduction process. Since the conduction at higher temperatures is predominantly due to electron hopping between $Fe^{3+} \leftrightarrow Fe^{2+}$ pairs, the activation energy is lower because of the higher mobility of electrons. But it is not understood why the activation energy for sample *B* is higher in the high temperature region which is distinct from the other three samples.

Usually a high conductivity is associated with small activation energy.[1] But in the present study this rule is not obeyed. For example, sample *A* exhibits a higher conductivity along with a higher activation energy whereas sample *B* shows a lower conductivity associated with a smaller activation energy. As discussed in Sec. III F, because of the frustrated topology arising from cationic disorder, it is possible that sample *A* exhibits higher activation energy for conduction. Sample *B* might have a lower degree of frustration because of thermal annealing and hence a lower activation energy for conduction.

C. Conduction mechanism

To study the relative contributions of holes and electrons to the conductivity, we determined the capacitance of the sample for various bias voltages. Figures 5(a) and 5(b) show the plot of $1/C^2$ versus bias voltage for samples *A* and *D* measured both at room temperature and at 673 K. For sample *A* at room temperature, $1/C^2$ curve has a positive slope at lower bias voltages and it becomes flat at higher bias voltages. The initial increase at lower bias voltages suggests that the conduction mechanism is predominantly due to hole hopping and the flat region at higher bias voltages indicates that electrons also contribute significantly to the conductivity. This explains why the activation energy is higher at low temperatures and it is lower at high temperatures. At high temperature (673 K), on the other hand, the curve is almost flat for all bias voltages, which reveals that both electrons and holes contribute almost equally to conductivity. But for sample *D*, the curve is almost flat for both at room temperature and high temperatures which suggests that both electrons and holes contribute to conductivity. However, it is yet to be understood why the difference in the two activation energies decreases for samples *C* and *D*. With more Co^{2+} ions on *B* sites in these two samples compared to that in sample *A*, there should be relatively an increase in the number of holes contributing to conduction and hence the difference in the two activation energies should not decrease.

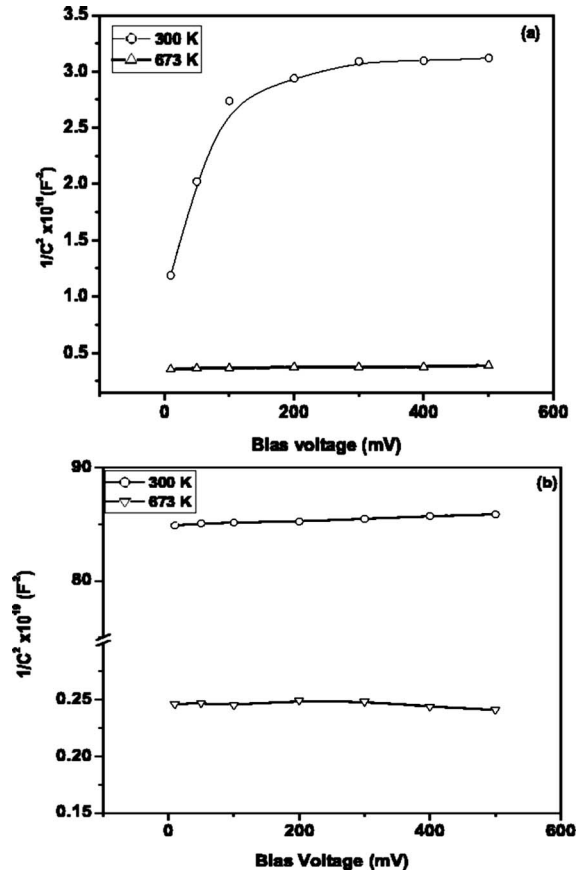

FIG. 5. $1/C^2$ vs bias voltage plot of $CoFe_2O_4$, (a) for sample *A* and (b) for sample *D*. The continuous line is a guide to the eye.

D. Dielectric relaxation

Figure 6 shows the plot of hopping frequency versus temperature. The hopping frequency refers to the dipolar orientational relaxation frequency. The temperature dependence of the dielectric relaxation frequency ω_p is written in the following form:

$$\omega_p = \omega_0 \exp\left(\frac{-E_p}{k_B T}\right), \tag{2}$$

where ω_0 is the preexponential factor, E_p is the activation energy for dielectric relaxation, and k_B is Boltzmann constant. The increase in relaxation frequency with temperature

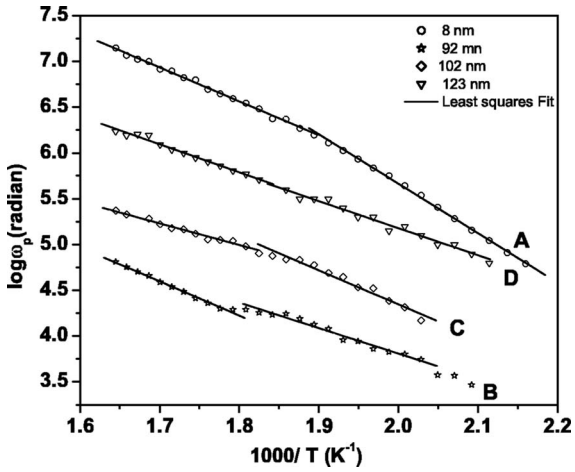

FIG. 6. The temperature dependence of the dielectric relaxation frequency ω_p of the $CoFe_2O_4$ samples. The solid lines are the best fit to Eq. (2).

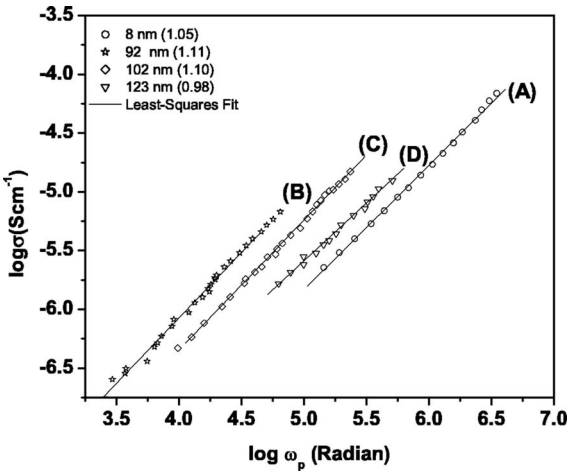

FIG. 7. $\log_{10}\sigma_{dc}$ vs $\log_{10}\omega_p$ plots (BNN relation) for nanocrystalline $CoFe_2O_4$. The solid lines are the least-squares fits. The values of the slopes are given in the parentheses.

is due to the thermal activation of the localized electric charge carriers forming dipoles, which are responsible for the dielectric polarization.[27] The activation energy E_p for the dielectric relaxation was calculated for various grain sizes from the slope of the straight lines shown in Fig. 6 and the values for various grain sizes are presented in Table I. Since the activation energy for dc conductivity (E_a) is almost equal to that for the dielectric relaxation (E_p), the same mechanism well occurs for both dc conductivity and dielectric relaxation.

E. BNN relation

Barton, Nakajima, and Namikawa[28] (BNN) have found the following relation to be valid for most of the electronically conducting disordered materials:

$$\sigma_{dc} = \frac{1}{4\pi H_R}\varepsilon_0 \Delta\varepsilon\omega_p, \tag{3}$$

where H_R is the Haven ratio, which indicates the degree of correlation between successive hops, ε_0 is the permittivity of free space, $\Delta\varepsilon=[\varepsilon(0)-\varepsilon(\infty)]$ is the change in permittivity from the unrelaxed baseline $[\varepsilon(\infty)]$ to the fully relaxed state $[\varepsilon(0)]$, and ω_p is the hopping frequency. The BNN relation is useful to find out whether ac and dc conductions are closely correlated to each other and whether the mechanism is the same for both. In order to find whether the BNN relation is obeyed or not, in nanocrystalline $CoFe_2O_4$ samples, we have plotted $\log_{10}\sigma_{dc}$ versus $\log_{10}\omega_p$ in Fig. 7 for all the four samples. The values of σ_{dc} and ω_p were obtained from the best fits from the nonlinear least-squares fitting. The solid lines result from the fitting and their slopes are almost equal to unity and this conveys that the dc and ac conductions are correlated to each other and that they are governed by the same mechanism.

F. Mössbauer studies

Mössbauer spectra (not shown here) were recorded at 298 K for all the four samples. But these spectra did not allow us to estimate accurately the proportions of Fe^{3+} ions in different sites, due to the lack of resolution of the hyperfine structure. In order to find the changes in the cation distribution of $CoFe_2O_4$ with heat treatment, we have therefore, recorded the in-field ^{57}Fe Mössbauer spectra for all the samples which are shown in Fig. 8. The Mössbauer spectra were fitted with two magnetic components arising from the tetrahedral (A) and octahedral site (B) Fe^{3+} ions. The experimental data have been fitted by using the least-squares MOSFIT program.[29] The refined values of hyperfine parameters are listed in Table II. In Table II, $\langle B_{eff}\rangle$ represents the algebraic sum of the internal hyperfine magnetic field and the external applied magnetic field. The sextet with the smaller value of isomer shift of 0.34 mm/s is unambiguously assigned to the tetrahedral Fe^{3+} ions, and the other one to the octahedral Fe^{3+} ions. The relative intensities of the A-site and B-site sextets obtained from the fitting of the in-field Mössbauer spectra are reliable as the spectra of the two sites are now well resolved. It was assumed that both sites have the same value for the f factor. The ratio of the intensity of the A-site sextet to that of the B-site sextet is expected to be 1.00, which is the ratio of the population of the Fe^{3+} ions in A sites to that in B sites, provided Co^{2+} ions are only in the B sites as observed in bulk sized particles. But the experi-

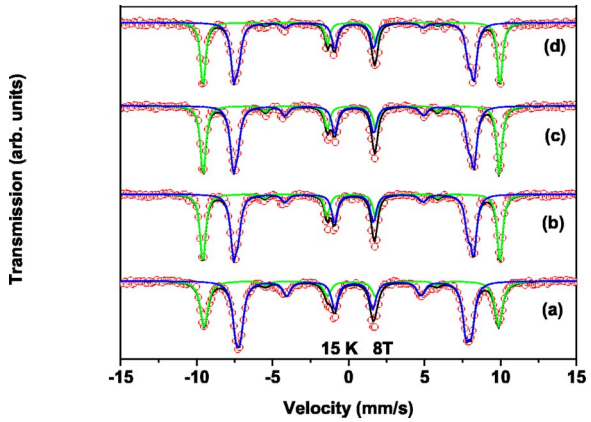

FIG. 8. (Color online) 8 T in-field Mössbauer spectra of the $CoFe_2O_4$ spinel ferrite for different grain sizes. (a) sample A (8 nm), (b) sample B (92 nm), (c) sample C (102 nm), and (d) sample D (123 nm).

TABLE II. Mössbauer parameters: Isomer shift $\langle IS\rangle$, quadrupole shift $\langle 2\varepsilon\rangle$, effective hyperfine field $\langle B_{\mathrm{eff}}\rangle$ (algebraic sum of the internal hyperfine magnetic field and the external applied magnetic field), hyperfine field $\langle B_{\mathrm{hyp}}\rangle$, canting angle $\langle\beta\rangle$, and relative intensity of the sextets $\langle I_{\mathrm{rel}}\rangle$ for the $CoFe_2O_4$ samples at 12 K in an external magnetic field of 8 T applied parallel to the direction of gamma rays.

Sample (grain size in nm)	Fe site	$\langle IS\rangle$[a] (mm/s) ±0.01	$\langle 2\varepsilon\rangle$ (mm/s) ±0.02	$\langle B_{\mathrm{eff}}\rangle$ (T) ±0.5	$\langle B_{\mathrm{hyp}}\rangle$ (T) ±0.5	$\langle\beta\rangle$ (degrees) ±5	I_{rel} (%) ±1
A	*A*	0.34	−0.00	59.8	52.3	20	36
(8)	*B*	0.49	−0.02	46.7	53.9	29	64
B	*A*	0.34	0.01	60.3	52.7	17	42
(92)	*B*	0.50	−0.03	49.0	56.5	22	58
C	*A*	0.34	−0.01	60.2	52.8	20	42
(102)	*B*	0.50	−0.06	48.1	55.5	24	58
D	*A*	0.36	−0.02	60.3	52.5	13	40
(123)	*B*	0.52	−0.02	48.0	55.6	18	60

[a]With respect to α-Fe at 300 K.

mental values obtained from the intensities of the *A*- and *B*-site sextets are 0.56, 0.72, 0.72, and 0.68 for samples with 8, 92, 102, and 123 nm grain sizes, respectively. The relative intensity of the *A*-site sextet is found to increase from sample *A* to sample *B*, which is possible only if some of the Fe^{3+} ions from the octahedral sites migrate to the tetrahedral sites on thermal annealing at 1473 K for 2 h. However, the relative intensity does not change by further increasing the annealing time, indicating that the cation distribution does not change with the duration of annealing at this temperature. The degree of inversion is the lowest for the as-prepared sample and it increases with annealing at 1473 K. However, the duration of annealing does not seem to have any influence on the degree of inversion. The nonvanishing intensity of the second and fifth lines in the two sextets of the Mössbauer spectra shows the presence of noncollinear spin structure. The average canting angle β defined as the angle between the direction of effective hyperfine field and the direction of applied magnetic field (γ-ray direction) was estimated and their values are listed in Table II. One notes that the mean canting angle slightly decreases when both the degree of cationic inversion and the grain size increase. Because of the size of present particles, one can exclude that the canted structure might result from the surface anisotropy. Indeed, when the particle exceeds about 10 nm diameter, the role of the surface on the magnetic properties can be neglected.[30,31] Even though we can expect that the surface spin anisotropy may contribute, to some extent, to the spin canting for the 8 nm particles, the observed spin canting for the higher grain sizes should be due to some other mechanism. The cationic inversion between Fe^{3+} and Co^{2+} does originate a magnetic frustrated topology, giving rise to a noncollinear magnetic structure, because of the presence of antiferromagnetic Fe–O–Fe, Co–O–Co, and Fe–O–Co superexchange interactions. However, the increase of the cationic inversion with annealing alone cannot be responsible for the decrease of canting angle. Consequently, the evolution of the canted structure versus the annealing has to be attributed, in addition to the local anisotropy of Co^{2+} ions, to some defects and vacancies combined with cationic inversion, the positions of which are dependent on the annealing time. The migration of Co^{2+}, Fe^{3+}, and vacancies gives rise, thus, to different cationic topology favoring magnetic frustration of antiferromagnetic interactions. Larger annealing times are required to achieve an ideal inverse spinel structure.

G. EXAFS analysis

EXAFS measurements were carried out to study the local atomic environment around the Fe^{3+} and Co^{2+} cations and to study the difference in the cation distribution between the nanostructured cobalt ferrites with different grain sizes. A laboratory x-ray absorption spectrometer (Rigaku R-XAS Looper)[32] was used for these measurements. Figures 9(a) and 9(b) show the Fourier transformed EXAFS spectra at Fe and Co-K absorption edges, respectively, for the as-prepared (*A*) and the heat treated *C* and *D* samples. In spinel ferrites the *A*-*A* correlation distance is longer than the *B*-*B*. The EXAFS profile at Fe-*K* edge for the bulk reference sample clearly shows two peaks in second nearest neighbor region, which is

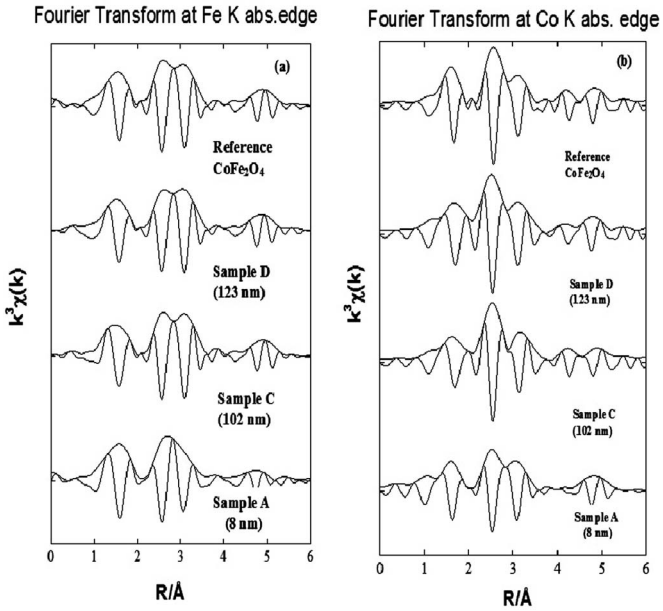

FIG. 9. (a) Fourier transforms of EXAFS spectra at Fe *K* absorption edge of $CoFe_2O_4$ ferrite samples. (b) The Fourier transforms of EXAFS spectra at Co *K* absorption edge of $CoFe_2O_4$ ferrite samples.

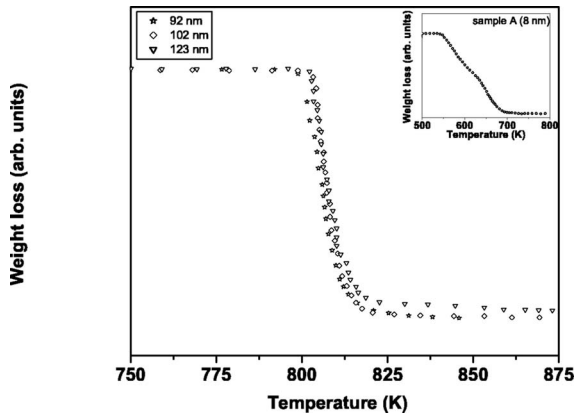

FIG. 10. Thermogravimetric plot of the $CoFe_2O_4$ spinel ferrite for different grain sizes.

a clear indication of the presence of Fe atoms in both octahedral and tetrahedral sites. One could also note nearly an equal intensity for both peaks, indicating an almost inverse structure of bulk cobalt ferrite. A similar profile could be observed for samples *C* (102 nm) and *D* (123 nm). But the EXAFS spectrum for the as-prepared sample *A* (8 nm) is quite different from others. There is a clear reduction in the intensity of the farther peak corresponding to the *A*-*A* correlation. From the EXAFS spectrum at Fe-*K* edge one could conclude that Fe^{3+} ions are not equally distributed between the octahedral and tetrahedral sites and relatively there are more number of Fe^{3+} ions in *B* sites than in *A* sites in the as-prepared sample. Thermal annealing thus induces some Fe^{3+} ions to migrate from the octahedral to tetrahedral sites as confirmed by the Mössbauer studies also.

The EXAFS profile at Co *K* edge for the bulk reference sample exhibits two distinct peaks in second nearest neighbor region, and their relative intensity is almost the same for the reference standard and samples *C* and *D*. But the relative intensity of the farther correlation peak is higher in the case of as-prepared sample (*A*), implying that there are more number of Co^{2+} ions in *A* site in sample *A* compared to that in other samples. From the EXAFS spectrum at Co-*K* edge, therefore, it is clear that the as-prepared sample has the lowest degree of inversion and that the degree of inversion increases with annealing as some of the Co^{2+} ions migrate from *A* to *B* sites on thermal annealing.

H. Néel temperature measurements

Figure 10 shows the thermogravimetric plots of $CoFe_2O_4$ obtained by using a thermogravimetric analyzer (TGA) with a small applied magnetic field of 4 mT. The instrument was calibrated with standard Ni and Fe samples by the two-point calibration method. The Néel temperature (T_N) is found to increase from 709 K (inset to Fig. 10) for the as-prepared sample (sample *A*) to 813 K for the sample annealed at 1473 K for 10 h (sample *D*). The values for samples *B* and *C* are 809 and 808 K, respectively. The increase in Néel temperature of the annealed sample is due to the change in the cation distribution during heat treatment. The in-field Mössbauer and EXAFS studies show that there is a migration of some of the Fe^{3+} ions from the octahedral to tetrahedral sites on thermal annealing. The replacement of the Co^{2+} ions by the Fe^{3+} ions on the tetrahedral (*A*) sites, therefore, increases the strength of the super exchange interaction and hence the Néel temperature. The possible increase in the *A*–O–*B* bond angle during heat treatment can also strengthen the superexchange interaction.

IV. CONCLUSION

The electrical conductivity of nanostructured $CoFe_2O_4$ has been explained on the basis of hopping of holes (Co^{II} and Co^{III}) and electrons (Fe^{2+} and Fe^{3+}) as evident from the change in the slope of the Arrhenius plot at about a temperature 540±3 K, which indicates that there are two different thermally activated processes in the conduction mechanism. The ac and dc conductions are governed by the same mechanism since the BNN relation is obeyed in these ferrites. The in-field Mössbauer and EXAFS studies show that there is a migration of some of the Fe^{3+} ions from the octahedral to tetrahedral sites on thermal annealing, which explains the observed decrease in conductivity when the grain size is increased from 8 to 92 nm. The degree of inversion is found to be smaller for the as-prepared sample compared to that for the annealed samples. The Néel temperature is found to increase from 709 K for the as-prepared sample (*A*) to 813 K for the annealed sample (*D*) because of the increase of Fe^{3+} ion population in tetrahedral sites, which leads to an increase in superexchange interaction strength. This is a very rare study where the effect of grain size alone on the electrical conductivity could be obtained, by keeping the cation distribution constant.

ACKNOWLEDGMENTS

The partial financial assistances from UGC-SAP (Phase III) and DST, Government of India (Sanction No. SR/S5/NM-23/2002), and the fruitful discussion with Dr. G. Govindaraj, Dr. R. Murugaraj, and Dr. N. Ponpandian are acknowledged.

[1] N. Ponpandian, P. Balaya, and A. Narayanasamy, J. Phys.: Condens. Matter **14**, 3221 (2002).
[2] N. Sivakumar, A. Narayanasamy, N. Ponpandian, J.-M. Greneche, K. Shinoda, B. Jeyadevan, and K. Tohji, J. Phys. D **39**, 4688 (2006).
[3] B. Viswanathan, in *Ferrite Materials*, edited by B. Viswanthan and V. R. K. Murthy (Narosa, New Delhi, 1990).
[4] Y. Shi, J. Ding, and H. Yin, J. Alloys Compd. **308**, 290 (2000).
[5] J. Ding, Y. J. Chen, Y. Shi, and S. Wang, Appl. Phys. Lett. **77**, 3621 (2000).
[6] Y. Suzuki *et al.*, Appl. Phys. Lett. **68**, 714 (1996).
[7] Y. C. Wang, J. Ding, J. B. Yi, B. H. Liu, T. Yu, and Z. X. Shen, Appl. Phys. Lett. **84**, 2596 (2004).
[8] G. D. Rieck and J. J. M. Thijssen, Acta Crystallogr., Sect. B: Struct. Crystallogr. Cryst. Chem. **24**, 982 (1968).
[9] G. A. Sawatzky, F. Van Der Woude, and A. H. Morrish, J. Appl. Phys. **39**, 1204 (1968).
[10] J. G. Na, T. D. Lee, S. J. Park, Y. J. Tang, and H. L. Luo, IEEE Trans. Magn. **31**, 3970 (1995).
[11] R. Carey and E. D. Isaac, Proc. Phys. Soc. London **81**, 741 (1963).
[12] S. Foner, J. Appl. Phys. **29**, 443 (1958).
[13] D. R. Corenjo and A. Medina-Boudri, Physica B **320**, 270 (2002).
[14] C. N. Chinnasamy, B. Jeyadevan, K. Shinoda, K. Tohji, D. J. Djayaprawira, M. Takahashi, R. Justin Joseyphus, and A. Narayanasamy, Appl. Phys. Lett. **83**, 2862 (2003).
[15] V. Blaskov, V. Petkov, V. Rusanov, Ll. Martinez, B. Martinez, J. S.

Muñoz, and M. Mikhov, J. Magn. Magn. Mater. **162**, 331 (1996).
[16]E. J. Choi, Y. Ahn, S. Kim, D. H. An, K. U. Kang, B.-G. Lee, K. S. Baek, and H. N. Oak, J. Magn. Magn. Mater. **262**, L198 (2003).
[17]M. Grigorova *et al.*, J. Magn. Magn. Mater. **183**, 163 (1998).
[18]H. H. Hamdeh, W. M. Hikal, S. M. Taher, J. C. Ho, N. P. Thuy, O. K. Quy, and N. Hanh, J. Appl. Phys. **97**, 064310 (2005).
[19]C. N. Chinnasamy, M. Senoue, B. Jeyadevan, O. Perales-Perez, K. Shinoda, and K. Tohji, J. Colloid Interface Sci. **263**, 80 (2003).
[20]C. N. Chinnasamy, B. Jeyadevan, O. Perales-Perez, K. Shinoda, K. Tohji, and A. Kasuya, IEEE Trans. Magn. **38**, 2640 (2002).
[21]G. H. Jonker, J. Phys. Chem. Solids **9**, 165 (1959).
[22]J. G. Na, T. D. Lee, and S. J. Park, IEEE Trans. Magn. **28**, 2433 (1992).
[23]J. G. Na, M. C. Kim, T. D. Lee, and S. J. Park, IEEE Trans. Magn. **29**, 3520 (1993).
[24]Z. Wu, Z. Bao, L. Cao, C. Liu, Q. Li, S. Xie, and B. S. Zou, J. Appl. Phys. **93**, 9983 (2003).
[25]B. D. Cullity, *Elements of X-ray Diffraction* (Addison Wesley, California, 1978).
[26]R. P. Mahajan, K. K. Patankar, M. B. Kothale, S. C. Chaudhari, V. L. Mathe, and S. A. Patil, Pramana, J. Phys. **58**, 1115 (2002).
[27]L. G. Van Uitert, J. Chem. Phys. **23**, 1883 (1995).
[28]H. Namikawa, J. Non-Cryst. Solids **18**, 173 (1975).
[29]J. Teillet and F. Varret, computer code MOSFIT (Université du Maine, Le Mans, France).
[30]E. Tronc, P. Prené, J. P. Jolivet, J. L. Dormann, and J. M. Greneche, Hyperfine Interact. **112**, 97 (1998).
[31]E. Tronc *et al.*, J. Magn. Magn. Mater. **221**, 63 (2000).
[32]T. Taguchi, J. Harada, K. Tohji, and K. Shinoda, Adv. X-Ray Anal. **45**, 397 (2002).